

AperTO - Archivio Istituzionale Open Access dell'Università di Torino

A 10,000 yr record of high-resolution Paleosecular Variation from a flowstone of Rio Martino Cave, Northwestern Alps, Italy

This is the author's manuscript

Original Citation:

Availability:

This version is available <http://hdl.handle.net/2318/1657670> since 2018-06-25T09:53:18Z

Published version:

DOI:10.1016/j.epsl.2017.12.047

Terms of use:

Open Access

Anyone can freely access the full text of works made available as "Open Access". Works made available under a Creative Commons license can be used according to the terms and conditions of said license. Use of all other works requires consent of the right holder (author or publisher) if not exempted from copyright protection by the applicable law.

(Article begins on next page)

1 **A 10,000 yr record of high-resolution Paleosecular Variation from a flowstone of**
2 **Rio Martino Cave, Northwestern Alps, Italy**

3
4 Elena Zanella¹, Evdokia Tema¹, Luca Lanci², Eleonora Regattieri^{3,4}, Ilaria Isola⁵, John C. Hellstrom⁶,
5 Emanuele Costa¹, Giovanni Zanchetta^{5,7}, Russell N. Drysdale^{8,9}, Federico Magri¹⁰

6 ¹Dipartimento di Scienze della Terra, Via Valperga Caluso 35, 10125 Torino, Italy

7 ²Dipartimento di Scienze Pure e Applicate, Piazza della Repubblica 13, 61029 Urbino, Italy

8 ³Institute of Geology and Mineralogy, University of Cologne, Zùlpicher Str. 49a, 50674 Cologne, Germany

9 ⁴Istituto di Geoscienze e Georisorse IGG-CNR, via Moruzzi 1, 56100 Pisa, Italy

10 ⁵Istituto Nazionale di Geofisica e Vulcanologia INGV, Via della Faggiola 32, 56126 Pisa, Italy

11 ⁶School of Earth Sciences, University of Melbourne, Victoria 3010 Australia

12 ⁷Dipartimento di Scienze della Terra, Via S. Maria 53 56126 Pisa, Italy

13 ⁸School of Geography, University of Melbourne, Victoria 3010, Australia

14 ⁹EDYTEM, UMR CNRS 5204, Université de Savoie-Mont Blanc, 73376 Le Bourget du Lac cedex, France

15 ¹⁰Gruppo Speleologico Valli Pinerolesi GSVP, Club Alpino Italiano, Pinerolo, Italy

16
17 **Abstract**

18 Speleothems are potentially excellent archives of the Earth's magnetic field, capable of recording
19 its past variations. Their characteristics, such as the continuity of the record, the possibility to be
20 easily dated, the almost instantaneous remanence acquisition and the high time -resolution make
21 them potentially unique high-quality Paleosecular Variation (PSV) recorders. Nevertheless,
22 speleothems are commonly characterized by low magnetic intensities, which often limits their
23 resolution. Here we present a paleomagnetic study performed on two cores from a flowstone
24 from the Rio Martino Cave (Western Alps, Italy). U/Th dating indicates that the flowstone's

25 deposition covers almost the entire Holocene, spanning the period ca. 0.5-9.0 ka, while an
26 estimation of its mean growth rate is around 1 mm per 15 years. The flowstone is composed of
27 columnar calcite, characterized by a highly magnetic detrital content from meta-ophiolites in the
28 cave's catchment. This favourable geological context results in an intense magnetic signal that
29 permits the preparation and measurement of thin(~3 mm depth equivalent) samples, each
30 representing around 45 yr. The Characteristic Remanent Magnetization (ChRM), isolated after
31 systematic stepwise Alternating Field demagnetization, is well defined, with Maximum Angular
32 Deviation (MAD) generally lower than 10°. Paleomagnetic directional data allow the
33 reconstruction of the PSV path during the Holocene for the area. Comparison of the new data with
34 archeomagnetic data from Italian archeological and volcanic records and using the predictions of
35 the SHA.DIF.14k and pfm9k.1a global geomagnetic field models shows that the Rio Martino
36 flowstone represents an excellent recorder of the Earth's magnetic field during the last 9,000
37 years. Our high resolution paleomagnetic record, anchored by a high-quality chronology, provide
38 promising data both for the detection of short term geomagnetic field variations and for
39 complementing existing regional PSV curves for the prehistoric period, for which well-dated data
40 are still scarce.

41

42 **Keywords:** Paleosecular variation, Rock magnetism, Speleothem, Italy

43

44 **1. Introduction**

45 To investigate geomagnetic field behavior in the past and to explore its short-term features, high-
46 resolution records from globally distributed archives of different origin are necessary (Mandea and
47 Olson, 2009). For Paleosecular Variation (PSV) reconstructions, an ideal paleomagnetic record

48 should satisfy several requirements, such as having a stable remanent magnetization, being well
49 dated, offering a continuous record and presenting high-time resolution. Even though some Earth
50 materials may satisfy a number of these, the characteristics of continuity and high-resolution are
51 rarely coupled. Marine and lacustrine sediment sequences are best at ensuring continuous records
52 and have therefore been intensively studied to obtain geomagnetic data over long time scales (e.g.
53 Turner and Thompson, 1981; Rolph et al., 2004; Vigliotti, 2006). However, sometimes data
54 reliability may be questionable: the remanence acquisition mechanisms, the smoothing effects of
55 bioturbation, the inclination error and the remanence acquisition delay are just some of the
56 problems that may affect this kind of record. On the other hand, volcanic rocks and fired
57 archeological artifacts may preserve very reliable paleomagnetic data but they are highly
58 discontinuous in time. The age uncertainties of the volcanic products, as well as the lack of
59 continuity and the limited time extension of available *in situ* archeological baked clay structures,
60 restrict their use for high-resolution record studies.

61 Several research groups have studied speleothems for both PSV and paleoenvironmental
62 reconstructions (e.g. Latham et al., 1989; Lean et al., 1995; Openshaw et al., 1997; Osete et al.,
63 2012; Xie et al., 2013; Font et al., 2014; Jaqueto et al., 2016; Lascu et al., 2016), revealing their
64 high potential for magnetic and secular variation reconstructions (Lascu and Feinberg, 2011).
65 Paleomagnetic time series from speleothems, although still sparse, can provide excellent temporal
66 resolution if the speleothem has grown continuously and over a considerable age range, as, for
67 example, in the case of the Mexican stalagmite studied in the pioneering work of Latham et al.
68 (1986). The key features of speleothems are that they can grow continuously for 10^3 - 10^5 yr and
69 can be accurately dated by the uranium-series method (e.g. Richards and Dorale, 2003). They
70 normally show little or no secondary alteration, and are generally easy to orient and sample
71 (though with obvious consideration of natural heritage values).

72 Based on magnetic properties, the remanent magnetization of speleothems can be divided into
73 two main genetic forms, detrital (DRM) or chemical (CRM) (Lascu and Feinberg, 2011). Detrital
74 input can originate from flood or drip water sources (Openshaw et al., 1997; Fairchild et al., 2006).
75 Moreover, speleothems present the advantage of acquiring their magnetization rapidly after
76 formation, meaning that the registered magnetic remanence variations reliably reflect the PSV
77 path in the past. Nevertheless, these promising features are confounded by a speleothem's
78 generally low concentration of magnetic minerals, and thus their low magnetic signal, which limits
79 their use in magnetic studies. To bypass this problem, large samples have been commonly used in
80 paleomagnetic studies, but this reduces the time-resolution of the sample. Generally, a sample of
81 around 2 cm may average ca 100-4000 yr (Strauss et al., 2013) and thus the obtained SV time-
82 resolution is very low.

83 This paper reports the results of a paleomagnetic study performed on a flowstone sampled at Rio
84 Martino Cave (North Western Alps, Italy). The favourable geologic context of the cave, which is
85 mainly surrounded by meta-ophiolites, makes this flowstone very rich in detrital ferromagnetic
86 components, and thus an ideal geomagnetic field recorder due to its high magnetic remanence
87 properties. Although a high content of detrital material can compromise U/Th dating (Hellstrom,
88 2006), we have been able to produce a continuous, radiometrically-dated, directional SV record
89 for the area during the last ~10 kyr, at a sampling resolution averaging 45 yr. Comparison of the
90 new data with archeomagnetic data from Italian artifacts and volcanic rocks and using predictions
91 of global geomagnetic field models, shows that the Rio Martino flowstone represents an excellent
92 recorder of the Earth's magnetic field in the past and demonstrates the potential of speleothems
93 for PSV studies and for the investigation of short-term variations of the geomagnetic field.

94

95 **2. Geological setting and sampling**

96 Rio Martino Cave (44°42' N, 7°09' E) is located in the inner sector of the Western Alps (Northern
97 Italy), which consists of a range of continental and oceanic tectono-metamorphic units bounded
98 by major orogen-scale faulting (Balestro et al., 2014), and exhumed and stacked in the axial sector
99 (Fig. 1). The cave is developed within the Mesozoic carbonate cover of the Palaeozoic Dora Maira
100 (Balestro et al., 2013). This unit is overlain by the Monviso meta-ophiolite complex, a major
101 eclogized remnant of the Ligurian-Piedmont oceanic lithosphere, which in turn is tectonically
102 overlain by the Queyras Schistes Lustrés, interpreted as a fossil accretionary wedge.

103 The surface above the cave is overlain mainly by glacial deposits. The cave is located at 1530 m
104 a.s.l. on the right flank of the upper Po valley. It is a spring cave, ca. 3000 m long, with 200 m of
105 elevation difference, and is crossed by a small river with an average discharge of 50 l/s (maximum
106 200 l/s) (Badino and Chiri, 2005).

107 The presence of highly magnetized rocks in the cave's catchment (Fig. 1) and the strong magnetic
108 anomalies observed in the Monviso Massif area (Lanza and Meloni, 2006) could induce a magnetic
109 deflection effect in the area. To evaluate the possible effect exerted by the meta-ophiolitic masses
110 and to confirm that it does not exert a significant influence on the paleomagnetic sampling, we
111 used a triaxial fluxgate magnetometer to measure the geomagnetic field components outside and
112 next to the entrance, as well as inside the cave. The computed magnetic inclination values of 60.7°
113 outside the cave and 60.5° on the flowstone surface are fully comparable to the 2013 IGRF model
114 of 60.6° (<http://www.ngdc.noaa.gov/geomag-web>). Besides, outside the cave we performed some
115 orientation checks by using both the magnetic and the solar compass. The difference between the
116 two declinations was small, ranging from -5° to +2°. Such differences are insignificant and indicate
117 that any local magnetic effects on the paleomagnetic sampling can be considered negligible.

118 Two sampling campaigns were carried out to collect two cores from the same flowstone, which
119 has accumulated on the side of a seasonally active stream with a high-detrital content. The cores

120 were taken ~20-30 cm apart and drilled using an adapted electric-powered drill. The first core
121 (RMD1), sampled during a campaign in 2010, was not azimuthally oriented. The second core
122 (RMD8), sampled in 2013, was oriented *in situ* by magnetic compass and inclinometer (figure S1 in
123 the supplemental material). Each core was ca. 60 cm long and was drilled perpendicular to the
124 flowstone growth axis.

125 A quarter of each core was dedicated to paleomagnetic analysis. The investigated sub-samples
126 consisted of small slices, about 3 mm thick (varying from 2.5 to 4 mm), cut almost perpendicular to
127 the speleothem's growth direction. Slicing was performed using a very thin non-magnetic saw,
128 which ensured that only 1 mm of material was consumed during the cut. Following this systematic
129 sampling, we obtained 146 slices from RMD1 and 143 from RMD8. Each slice was positioned in the
130 centre of a non-magnetic plastic cylinder (2.5 cm diameter, 2.3 cm height) that allowed its
131 handling as per standard paleomagnetic samples (Fig. 2).

132

133 **3. Methods**

134 *3.1. U/Th dating and age modelling*

135 Nineteen solid prisms of ~40 mg (~2 mm wide along the lamina and 1 mm thick on growth axis)
136 from RMD1 were used for age determination (Table S1 in Supplementary Material). The U/Th
137 dating was performed at the University of Melbourne (Victoria, Australia) following the method of
138 Hellstrom (2003). Briefly, samples were dissolved and a mixed ^{236}U - ^{233}U - ^{229}Th spike was added
139 prior to removal of the carbonate matrix with ion-exchange resin. The purified U and Th fraction
140 was introduced in a dilute nitric acid to a multi-collector inductively coupled plasma mass
141 spectrometer (MC-ICPMS, Nu-Instruments Plasma). The $^{230}\text{Th}/^{238}\text{U}$ and $^{234}\text{U}/^{238}\text{U}$ activity ratios
142 were calculated from the measured atomic ratios using an internally standardised parallel ion-

143 counter procedure and calibrated against the HU-1 secular equilibrium standard. Correction for
144 detrital Th content was applied using initial activity ratios of detrital thorium ($^{230}\text{Th}/^{232}\text{Th}$)_i of $1.3 \pm$
145 0.45. This value, and its relative 2σ uncertainty, was calculated using a Monte Carlo 'stratigraphic
146 constraint' procedure based on the series of U/Th ages (Hellstrom, 2006). A depth-age model was
147 constructed using a Bayesian Monte Carlo approach following the method described by Drysdale
148 et al. (2005) and Scholz et al. (2012).

149 *3.2. SEM-EDS analysis*

150 The mineralogy of the detrital inclusions in the studied flowstone was investigated by dissolving
151 different portions of various thin slabs of the RMD1 core in diluted hydrochloric acid and passing
152 the digests through 0.45 micrometre cellulose acetate filters. The residues, bearing almost all of
153 the non-carbonate mineral inclusion types contained in the speleothem, were observed and
154 analysed with a Cambridge Stereoscan 360 Scanning Electron Microscope housed at the Earth
155 Science Department of the University of Torino, Italy. Analyses were performed using an Oxford
156 Inca X-Act 200 EDS microanalysis equipped with a Link Pentafet detector (thin window), allowing
157 qualitative/quantitative determination of light elements (down to boron). All data were obtained
158 at 15 kV HT, 25 mm WD, probe current range 800 pA – 1.2 nA and analysis time from 60 to 500 s.
159 Primary standardization was performed on SPI Supplies and Polaron Equipment standards, and the
160 system was regularly calibrated against a high-purity metallic Co standard before each
161 experimental session. Data were processed with the Inca 200 Microanalysis Suite Software,
162 version 4.08, and calibrated on natural mineral standards using the ZAF correction method.
163 Analytical data are considered to be only semi quantitative due to the nature of the samples
164 (rough surface of the particles, lack of horizontality, lack of surface polishing). A total of about
165 1500 analyses was performed on seven samples coming from different portions of the core,

166 corresponding to about 200 measurements for each filter, randomly scattered on the filter surface
167 for better representativeness.

168 Despite the results of magnetic analysis, very few magnetite particles were found in the filtered
169 material, most likely because the single-domain magnetic particles were not retained by the 0.45
170 μm filter. Magnetite was indeed observed in sandy materials from Rio Martino, being found in the
171 bed sediments of the relatively high-energy environment of the cave stream, rather than as
172 detritus in carbonate flowstone speleothems.

173

174 *3.3. Rock magnetic measurements*

175

176 All magnetic measurements were performed at the ALP Paleomagnetic Laboratory (Peveragno,
177 Italy). Rock magnetic experiments were performed on representative samples from both cores.
178 Rock magnetism was investigated by low-field susceptibility (k_m) and natural remanent
179 magnetization (J_r) measurements using a KLY3 kappabridge and a JR6 spinner magnetometer with
180 a sensitivity of the order of 10^{-8} SI and 10^{-6} A/m, respectively. Susceptibility was measured at least
181 five times *per* sample in order to calculate a mean value. Standard deviation is low and normally
182 less than 5% for specimens associated with a susceptibility spike; uncertainty grows to 20-35% for
183 the remaining specimens, characterized by negative (diamagnetic) susceptibility values. All
184 samples were weighed to get the mass-normalized susceptibility (χ , m^3kg^{-1}) and intensity (J ,
185 Am^2/Kg). Their values are represented as a function of the core depth in figure S2 of the
186 supplemental material.

187 Isothermal Remanent Magnetization (IRM) curves were obtained with an ASC pulse magnetizer,
188 applying stepwise increasing fields up to 1 T. Thermal demagnetization of a three-axis composite
189 IRM was also performed on representative samples (Lowrie, 1990). An IRM was imparted with an

190 ASC pulse magnetizer along the sample's three orthogonal axes, applying first a maximum 1.5 T,
191 then a medium 0.3 T and finally a minimum 0.1 T magnetic field. Crossover plots of IRM curves and
192 alternating field (AF) demagnetization of the saturation IRM (SIRM) were carried out to investigate
193 the magnetic grain size (Symons and Cioppa, 2000).

194 Finally, hysteresis cycles were obtained by a Vibrating Sample Magnetometer (VSM, LakeShore
195 7410 - Maximum applied field $B_{\max} = \pm 1$ T; $H = \pm 10.000$ Oe / 976.000 A/m) at the Istituto
196 Nazionale di Ricerca Metrologica (INRIM, Torino) and interpreted by RockMag Analyzer 1.0
197 software (Leonhardt, 2006). All specimens were AF demagnetized stepwise up to 100 mT with a
198 ASC-D 2000 equipment. Representative twin specimens were also stepwise thermally
199 demagnetized with a Schonstedt TSD-1 furnace.

200

201 **4. Results**

202 *4.1. Chronology*

203 All the U/Th ages obtained from RMD1 were in stratigraphic order within the associated
204 uncertainties, except for two samples that were consequently rejected as outliers (Table S1 in
205 Supplementary Material). Macroscopic and thin-section analyses of core RMD1 shows no growth
206 interruption along its length. Age modelling performed on RMD1 indicates that the flowstone
207 grew continuously between 0.56 ± 0.06 ka and 9.7 ± 1.6 ka b2k (Fig. 3). The mean growth rate is
208 0.058 mm/yr, which implies a mean time-resolution of ca. 60 yr (3 mm specimen + 1 mm cut) for
209 the PSV record. The time averaged in each 3 mm slice sample is ca. 45 yr. The age of RMD8 was
210 inferred by comparing clearly visible growth layers (Fig. 2a) between the two cores, associated
211 with spikes in both the magnetic mass susceptibility and mass magnetization (figure S2 of the
212 supplemental material).

213 4.2. EDS

214 The mineralogy of the detrital portion in the RMD1 core is in strong accord with the composition
215 of the surrounding lithology. Apart of the calcareous formation in which the cave has developed,
216 the main rocks in the area are prasinites, amphibolites and serpentines. Minerals were grouped by
217 similar chemistry, with some simplifications: as stated above, analyses were only semi-
218 quantitative. The main identified groups are: iron oxides (without magnetite, discriminated by
219 morphological features), magnesium silicates (other than serpentine), serpentine group, white
220 mica group, feldspar, tremolite-actinolite amphiboles, other amphiboles (mainly hornblende),
221 epidote group, chlorite group, quartz and accessories. The main minerals (Fig. 4) are represented
222 by iron oxides (not distinguishable by chemistry for the reason explained above), magnesium
223 silicates and serpentine group minerals. Iron oxides are mostly irregular in shape as if they had
224 undergone reworking from the stream or by feedwater (Perkins, 1996). In few cases, a framboidal
225 shape suggests *in situ* growth.

226

227 4.3. Magnetic mineralogy

228 The mass magnetic susceptibility of the specimens strongly varies. It mostly shows a prevailing
229 diamagnetic phase with small negative values (from -7 to $0 \times 10^{-9} \text{ m}^3 \text{ kg}^{-1}$ with a mean value of $-4 \times$
230 $10^{-9} \text{ m}^3 \text{ kg}^{-1}$), alternating with high positive spikes, up to $970 \times 10^{-9} \text{ m}^3 \text{ kg}^{-1}$, suggesting a very low
231 concentration of magnetic minerals in these specimens. Calcite bulk susceptibility is $-12.09 \mu\text{SI}$; its
232 mass susceptibility is about $-4.46 \times 10^{-9} \text{ m}^3 \text{ kg}^{-1}$ (Almqvist et al., 2010). Since the literature value for
233 the susceptibility of calcite refers to single crystal, we can assume that the mass susceptibility for
234 calcite in the speleothem is slightly higher, because of mineral porosity. Assuming a constant
235 diamagnetic contribution mostly due to calcite, the relative variability of magnetic susceptibility is

236 indicative of variations of the concentration of magnetic minerals: a mean χ value of $-4 \times 10^{-9} \text{ m}^3$
237 kg^{-1} can be assumed to be representative of the “standard” content in magnetite, while high
238 values represent for pulses of higher detrital input.

239 The natural magnetization intensity (J_r) strongly varies from specimen to specimen, being on
240 average around $1\text{-}10 \times 10^{-6} \text{ Am}^2 \text{ kg}^{-1}$ with spikes up to $80 \times 10^{-6} \text{ Am}^2 \text{ kg}^{-1}$. The variations of these
241 two bulk parameters are correlated; the computed correlation coefficients are $r = 0.87$ and $r =$
242 0.76 for RMD1 and RMD8, respectively. This corroborates the hypothesis that their values are
243 essentially controlled by changes in concentration of the magnetic oxide.

244 IRM acquisition curves from representative samples saturate at relatively low field (around 0.3 T),
245 indicating the presence of low coercivity minerals (Fig. 5a). The IRM acquisition data were further
246 analyzed applying the MAX UnMix software (Maxbauer et al., 2016) to six flowstone slices and to
247 sand collected from the bed of the cave spring. For three specimens, i.e. RM101 and RM134
248 flowstones and the sand, only one magnetic component was identified with Bh and DP values fully
249 consistent with detrital magnetite (Bh = 1.46, DP = 0.40). In the remaining cases, two components
250 were detected, one as above, and the other pointing to higher-coercivity magnetite. The
251 computed S-ratio ($S_{0.3 \text{ mT}}$) ranges from 0.95 to 1.00.

252 During the thermal demagnetization of the orthogonal IRM components (Lowrie, 1990), two
253 typical behaviors were observed, which are independent of the magnetization intensity of the
254 specimens. The first (e.g. sample RM68a), representing about the 80% of the measured
255 specimens, suggests that the primary remanence is dominated by a soft magnetic carrier,
256 demagnetized at ca 350-450 °C, which is interpreted as a titanomagnetite (Fig. 5b). The second
257 (e.g. sample RM44a), in the remaining 20%, is characterized by a first drop in the magnetization
258 intensity between 200 and 300 °C, which may be speculatively related to the existence of
259 maghemite (Pan et al., 2000), even though this evidence is not sufficient to unambiguously

260 identify this magnetic phase (Zhu et al., 2012). The presence of (titano)magnetite of detrital origin
261 is easily justified considering the geologic context of the cave and it is probably originated from
262 the highly magnetic rocks of the surrounding area, mostly meta-ophiolites (Balestro et al., 2013).
263 The occurrence of small serpentinite lithics was also detected. In those cases, the Median
264 Destructive Field (MDF), which is normally stable and around 50-60 mT, drops to 5-25 mT.
265 Deflections from $MDF = 50$ mT occur only where both the magnetic susceptibility and the
266 magnetization intensity values are high. To check for these variations, we performed the
267 experiment of Symons and Cioppa (2000) on some selected specimens, which were characterized
268 by MDF ranging from 15 to 60 mT. It consists of a crossover plot, where the %SIRM is plotted as a
269 function of the applied field, and using a logarithmic scale (Fig. 5c). The results suggest that,
270 except specimen SP212, which is characterized by MD (titano)magnetite, samples mainly contain
271 SD to PSD (titano)magnetite grains.

272 The modified Lowrie-Fuller method (Johnson et al., 1975), which represents a valid first-order
273 indicator of grain-size composition (Font et al., 2014), was applied to some specimens with MDF in
274 the range 45-50 mT. Results always show L-type behaviors with the Anhyseretic Remanent
275 Magnetization (ARM) dominating the Isothermal Remanent Magnetization (IRM) during AF
276 demagnetization treatment, corroborating the occurrence of SD grains.

277 These results are confirmed by the hysteresis cycles (Figure S3 in the supplemental material)
278 performed on 2 specimens, one characterized by high χ , one by low χ . After correction for the
279 diamagnetic effect, the curves show the occurrence of a low-coercivity phase with saturation at
280 0.3-0.5 T; in both cases, the ratios M_{rs}/M_s and B_{cr}/B_c fall next to the PSD field and SD + MD mixing
281 curve in the Day plot (Dunlop, 2002).

282 **5. Paleomagnetic directions**

283 *5.1. Natural Remanent Magnetization and the Anisotropy of Remanent Magnetization*

284 Speleothems can potentially offer very useful records of PSV and the remanence acquisition
285 mechanisms in speleothems have been previously studied in detail (e.g., Lascu and Feinberg, 2011;
286 Strauss et al., 2013, and reference therein). In order to provide a reliable PSV record, the
287 magnetization should be acquired and locked soon after the calcium carbonate film is deposited
288 on a speleothem (almost instantaneously). Following Strauss et al. (2013), lock-time for a
289 speleothem is sub-annual and the magnetization is a DRM. Synchronicity between crystallization
290 and magnetization has been tested experimentally by synthetic stalagmite growth (Morinaga et
291 al., 1989), confirming the short time-lapse in acquiring magnetization parallel to the ambient field
292 direction.

293 To test if this requirement is encountered in Rio Martino flowstone and thus to check for its
294 reliability as a PSV recorder, we measured both the Anisotropy of Magnetic Susceptibility (AMS)
295 and the Anisotropy of Isothermal Remanent Magnetization (AIRM) on two selected sets of
296 samples from RMD1 (azimuthally non-oriented core), each comprising a time interval of ca 1000
297 yr. The first set comprised 16 samples (SP200 to SP260) from 4.26 ± 0.23 to 3.30 ± 0.03 ka, and the
298 second set 14 samples (SP346 to SP397) from 7.76 ± 0.12 to 6.91 ± 0.11 ka. A difference of 20° in
299 the mean magnetic ChRM inclination distinguished these two sets of specimens. The AMS was
300 measured by a KLY-3 kappabridge. The results obtained on both sets of samples show a well-
301 defined (confidence angles $< 15^\circ$) mean minimum susceptibility axis, k_3 , which is statistically
302 vertical and perpendicular to the flowstone growth laminae (Fig. 6a). For the AIRM measurements,
303 each specimen was first AF demagnetized using a tumbling 2G demagnetizer at 60 mT peak field
304 and then given an isothermal remanent magnetization (IRM) with a steady field of 20 mT using an
305 AGICO PUM-1 pulse magnet. After measurement with the spinner magnetometer, the sequence
306 was repeated for a total of 12 different orientations of the IRM in order to calculate the anisotropy
307 tensor. The experiment (Fig. 6b-c) shows that for both sets, the maximum IRM anisotropy axis I_1 is

308 concordant or statistically indistinguishable from the mean ChRM direction, showing no relation
309 with the speleothem growth laminae. This shows that ChRM direction is due to the statistical
310 alignment of the magnetic particle and fully agrees with the conclusions of Zhu et al. (2012), who
311 performed both AMS and AIRM on stalagmites. They found that the AMS was dominated by the
312 calcite fabric, being the minimum susceptibility axis k_3 aligned perpendicular to the stalagmite
313 growth laminae, while the AIRM fabric showed the maximum remanence axis I_1 almost parallel to
314 the NRM direction. These data all point to a detrital origin of the magnetization, with the
315 geomagnetic field control in the orientation of the ferromagnetic minerals.

316

317 *5.2. Characteristic Remanent Magnetization determination*

318 Demagnetization results are represented by intensity-decay curves and plotted in Zijderveld
319 diagrams (Fig. 7). Most of the specimens are characterized by a small viscous remanent
320 magnetization (VRM), which is easily removed at an AF field of 15-20 mT. The remaining
321 demagnetization path is linear and points to the origin, indicating a stable remanent
322 magnetization; this component has been interpreted as the Characteristic Remanent
323 Magnetization (ChRM). The ChRM direction is mostly well defined and characterized by low MAD
324 values (lower than 8° for the 91% of the studied samples). AF and thermal demagnetization results
325 obtained from twin specimens are very similar (Fig. 7), confirming the reliability of the ChRM
326 direction (Fig. 8; Table S2 in Supplementary Material). In the thermal demagnetization (Fig. 7b and
327 7d), an inflection in the intensity decay curve it is observable at ca. 150 °C. As suggested by Strauss
328 et al. (2013) the decay could be correlated with the occurrence of goethite, not detected however
329 by any other experiment. The AF demagnetization treatment has been preferred rather than the
330 thermal demagnetization, as it permits the further use of the same samples for
331 paleoenvironmental and relative paleointensity investigations through Anhyseretic Remanent

332 Magnetization (ARM) measurements. Therefore, all samples were systematically AF demagnetized
333 and ChRM directions were obtained from the AF demagnetization results. Demagnetization
334 behavior in samples with low- and high-remanence (spike) does not change significantly except for
335 specimens where serpentinite clasts were recognized.

336

337 **6. Directional Paleosecular Variation during Holocene**

338 Paleomagnetic directions obtained from the two cores (reported in Table S2 of Supplementary
339 material) are plotted versus depth from the top of the core in Figure 9. Some spikes in declination
340 show a strong correspondence with atypical MDF values, lower/higher than 20/60 mT. These
341 deflected directions have been ascribed to the presence of small serpentinite lithic fragments and
342 were thus rejected. The declination of RMD1, which was not azimuthally oriented, has been
343 recovered after adjustment of its mean value to the Geocentric Axial Dipole (GAD) calculated at
344 Rio Martino according to the following procedure: first, the mean direction of RMD1 has been
345 calculated for the last 10 kyr and then its deviation from the GAD value has been computed. The
346 difference in declination between the core and the GAD has been extracted from each declination
347 value of the RMD1 core.

348 Generally, directions obtained from both RMD1 and RMD8 are in good agreement with each other
349 and data reproducibility is high (Fig. 9). This is particularly evident for the inclination data at
350 depths between 200.0 and 600.0 mm, where the two records match each other. Instead, in some
351 cases, mostly at depths from 150.0 to 200.0 mm, differences in inclination of around 20°-25° are
352 observed. The cause of such differences is not clear, even though uncertainties during sampling
353 (slices not perfectly perpendicular to the flowstone growth) and deflections related to a possible
354 anisotropy effect connected to the calcite crystals growth cannot be completely excluded. To

355 guarantee the high quality of the new data, only ChRM directions characterized by MAD values
356 lower than 6° have been used in the plots. Directional data of each core have been kept clearly
357 distinguishable, because only RMD1 was directly dated and even though the paleomagnetic
358 records from the two cores are consistent and despite the fact that the two cores are only 30 cm
359 apart, their simultaneous growth cannot be fully guaranteed.

360 The paleosecular variations registered by the Rio Martino speleothem are compared with spot
361 archeomagnetic directions obtained from dated archeological structures and volcanic rocks from
362 Italy. The data from the *in situ* archeological material are taken from the Italian archeomagnetic
363 dataset (Tema et al., 2006; Tema, 2011) updated by some recently published results (Malfatti et
364 al., 2011; Kapper et al., 2014; Tema et al., 2013; 2015; 2016). The data from the Italian volcanic
365 eruptions have been downloaded from the GEOMAGIA50.v3 database (Brown et al., 2015). All
366 data have been relocated at the geographic coordinates of Rio Martino via the virtual geomagnetic
367 pole method (Noel and Batt, 1990). The comparison shows that the archeomagnetic and volcanic
368 data generally fit very well to the speleothem directions (Fig. 10). Some discrepancies in
369 declination can be observed around 1000 AD. For this period the speleothem declination values
370 are very low and quite dispersed. Nevertheless, it is particularly interesting to note that for the BC
371 period, the available archeomagnetic data, even if very limited and often accompanied by large
372 error bars, are in excellent agreement with the new data, in spite of the speleothem inclination
373 being systematically higher. Recently, Ponte et al. (2016) noticed that the inclination values in
374 speleothems seem to vary as a function of the orientation of the calcite growth. To check for this
375 effect, we calculated the mean paleomagnetic direction for both RMD1 and RMD8 applying Fisher
376 Statistics, selecting ChRMs with $MAD < 6^\circ$. Their mean directions (RMD1: $D = 358.8^\circ$, $I = 65.1^\circ$, α_{95}
377 $= 1.9^\circ$; RMD8: $D = 2.4^\circ$, $I = 65.8^\circ$, $\alpha_{95} = 1.7^\circ$) are close to the GAD at Rio Martino's geographic
378 coordinate ($D = 0^\circ$, $I = 63^\circ$), even if statistically distinguishable. However, AIRM shows a reliable

379 consistency between the mean ChRM and the mean I_1 axis, which confirms that the orientation of
380 the ferromagnetic minerals was mainly controlled by the geomagnetic field present during
381 speleothem accumulation. This substantiates the high potential of Rio Martino speleothems to
382 continuously and reliably register the Earth's magnetic field, offering a unique source of high
383 quality data for the BC period where *in situ* archeological artifacts are very scarce.

384 The new data are also compared with the predictions of global geomagnetic field models. Here,
385 we have used for comparison the pfm9k.1a (Nilsson et al., 2014) and the SHA.DIF.14k (Pavón-
386 Carrasco et al., 2014) models that are the most recently published global geomagnetic models for
387 the Holocene. There is good agreement between the speleothem records and the global models
388 predictions, confirming some interesting features of the Earth's magnetic field in the past. The
389 eastward declinations around 1000 BC mainly observed in the SHA.DIF.14k model are observed in
390 the speleothem data for the same time period, and also show high declination values. For the
391 4000-2000 BC period, only small declination variations are shown by the speleothem data, in
392 agreement with the pfm9k model's predictions, while the declination peaks seen in the
393 SHA.DIF.14k model (e.g. around 3600 BC) are not confirmed by the speleothem data. For periods
394 older than 5000 BC, speleothem records show generally higher declination values compared to the
395 model predictions and other archeomagnetic data. Interestingly, similar eastward declination
396 values were found for cave sediments in Switzerland (Kapper et al., 2014). Regarding the
397 inclination data, good agreement can be observed for the periods 6000-3500 BC and 500 BC-500
398 AD. However, around 1000 BC, speleothems show an interesting high-inclination peak that is not
399 observed in the models or sustained by the available archeomagnetic data. This peak is actually
400 only observed on the data from the RMD8 core and definitely more independent records are
401 necessary to investigate if it corresponds to a real abrupt directional change (as it corresponds also
402 to high declination values) of the geomagnetic field at this time period. For the 7500 BC to 6000 BC

403 period, the speleothem records show continuously increasing inclination with a peak around 6000
404 BC that seems to be in agreement with the model's predictions.

405

406 **7. Conclusions**

407 Some outstanding characteristics of the Rio Martino flowstone, such as its continuous growth, the
408 well-constrained chronology and the intense magnetic signal, make its paleomagnetic directional
409 record for the Holocene in the northwestern Italy particularly appropriate for PSV investigation.
410 The high magnetic signal permits a high-resolution record of around 60 yr per data point; the
411 regular scatter of paleomagnetic data through time shows an almost constant distribution of
412 directional data though the Holocene.

413 The obtained directional results are well defined and offer a unique, almost continuous, secular
414 variation record for the last ~10,000 years. Although some discrepancies can be observed,
415 comparison with archeomagnetic data and global geomagnetic field models confirms the high
416 potential of these speleothems to the reconstruction of the Earth's magnetic field variations in the
417 past.

418 Our results show that the Rio Martino flowstones are not affected by recrystallization effects or
419 secondary alterations. The speleothems do not show any inclination shallowing when compared
420 with model predictions, and in some cases show high inclination peaks that are not observed by
421 the models (e.g. around 3800 BC, 1000 BC, 800 AD).

422 The record characteristics overcome some typical features affecting both clastic sedimentary and
423 the archeomagnetic PSV records, including the smoothness of the magnetic data in the case of the
424 former and the presence of temporal gaps and uneven data distribution in the case of the latter.

425 The high resolution obtained points to the possibility of detecting short and abrupt geomagnetic
426 field changes by studying a wide variety of Earth Magnetic Field variations at a timescale from tens

427 of years to the millennia and highlights the importance of regional differences when modelling the
428 Earth's field. The use of speleothem records for PSV reconstructions can be particularly important
429 for the prehistoric period where other sources of data coming from archeological artifacts or well-
430 dated volcanic eruptions are scarce.

431

432 **Acknowledgments**

433 We thank the Associazione Gruppi Speleologici Piemontesi (AGSP) for the logistical support during
434 field campaign and in particular Raffaella Zerbetto for her kindness and competence. E. Ferrara
435 (INRIM) is gratefully acknowledged for hysteresis measurements and A. Roncioni for his support in
436 coring operations. J.M. Feinberg and two anonymous referees are thanked for helpful reviews that
437 greatly improved the manuscript. This paper is dedicated to the memory of Prof. Roberto Lanza
438 who enthusiastically supported this study during the last months of his life giving fundamental
439 advices and suggestions.

440 **References**

- 441 Almqvist, B.S.G., Herwegh, M., Schmidt, V., Pettke, T., Hirt, A.M., 2010. Magnetic susceptibility as a
442 tool to study deformed calcite with variable impurity content. *Geochemistry Geophysics*
443 *Geosystems*, 11, Q01Z09, doi:10.1029/2009GC002900
- 444 Badino, G., Chiri, M., 2005. First data from the underground meteorological station of Rio Martino,
445 Italy. *Hellenic Speleological Society*. 21-28 August 2005, Kalamos, Greece.
- 446 Balestro, G., Fioraso, G., Lombardo, B., 2013. Geological map of the Monviso massif (Western
447 Alps). *Journal of Maps*, 9, 4, 623-634, doi: 10.1080/17445647.2013.842507
- 448 Balestro, G., Festa, A., Tartarotti, P., 2014. Tectonic significance of different block-in-matrix
449 structures in exhumed convergent plate margins: examples from oceanic and continental HP

450 rocks in Inner Western Alps (northwest Italy). *International Geology Review*. DOI:
451 10.1080/00206814.2014.943307.

452 Brown, M.C., Donadini, F., Korte, M., Nilsson, A., Korhonen, K., Lodge, A., Lengyel, S.N., Constable,
453 C.G., 2015. GEOMAGIA50.v3: 1.General structure and modifications to the archeological and
454 volcanic database. *Earth Planets Space*, 67:83, doi:10.1186/s40623-015-0232-0

455 Drysdale, R.N., Zanchetta, G., Hellstrom, J.C., Fallick, A.E., Zhao, J.X., 2005. Stalagmite evidence for
456 the onset of the Last Interglacial in southern Europe at 129+/-1 ka. *Geophysical Research*
457 *Letters* 32, 1-4.

458 Dunlop, D.J., 2002. Theory and application of the Day plot (M_{rs}/M_s versus H_{cr}/H_c) 1. Theoretical
459 curves and tests using titanomagnetite data. *J. Geophys. Res.*, 107, 2056, doi:
460 10.1029/2001JB000486

461 Fairchild, I.J., Smith, C.L., Baker, A., Fuller, L., Spötl, C., Matthey, D., McDermott, F., 2006.
462 Modification and preservation of environmental signals in speleothems. *Earth Science*
463 *Reviews*, 75, 105-153, doi:10.1016/j.earscirev.2005.08.003

464 Font, E., Veiga-Pires, C., Pozo, M., Carvallo, C., de Siqueira Neto, A.C., Camps, P., Fabre, S., Mirão,
465 J., 2014. Magnetic fingerprint of southern Portuguese speleothems and implications for
466 paleomagnetism and environmental magnetism. *Journal of Geophysical Research*, 119,
467 7993-8020, doi:10.1002/2014JB011381.

468 Hellstrom, J.C., 2003. Rapid and accurate U/Th dating using parallel ion-counting multicollector
469 ICP-MS. *Journal of Analytical Atomic Spectrometry* 18, 1346-1351

470 Hellstrom, J.C., 2006. U-Th dating of speleothems with high initial ^{230}Th using stratigraphical
471 constraint. *Quaternary Geochronology*, 1, 289-295.

472 Jaqueto, P., Trindade, R.I.F., Hartmann, G.A., Novello, V.F., Cruz, F.W., Karmann, I., Strauss B.E.,
473 Feinberg, J.M., 2016. Linking speleothem and soil magnetism in the Pau d'Alho cave (central
474 South America). *Journal of Geophysical Research*, 121, doi:10.1002/2016JB013541.

475 Johnson, H.P., Lowrie, W., Kent, D.V., 1975. Stability of Anhysteretic Remanent Magnetization in
476 fine and coarse magnetite and maghemite particles. *Geophysical Journal of the Royal
477 astronomical Society*, 41, 1-10.

478 Kapper, L., Anesin, D., Donadini, F., Angelucci, D., Cavulli, F., Pedrotti, A., Hirt, A., 2014. Linking site
479 formation processes to magnetic properties. Rock and archaeomagnetic analysis of the
480 combustion levels at Riparo Gaban (Italy). *Journal of Archaeological Science*, 41, 836-855.

481 Kapper, L., Donadini, F., Mauvilly, M., Panovska, S., Hirt, A.M., 2014. New directional
482 archaeomagnetic data of burned cave sediments from Switzerland and geomagnetic field
483 variations in Central Europe. *Geophysical Journal International*, 198, 1208-1221,
484 doi:10.1093/gji/ggu184

485 Lanza, R., Meloni, A., 2006. *The Earth's Magnetism. An Introduction for Geologists*. Springer, 278
486 pp.

487 Lascu, I., Feinberg, J.M., 2011. Speleothem magnetism. *Quaternary Science Reviews*, 30, 3306-
488 3320.

489 Lascu, I., Feinberg, J.M., Dorale, J.A., Cheng, H., Edwards, R.L., 2016. Age of the Laschamps
490 excursion determined by U-Th dating of a speleothem geomagnetic record from North
491 America. *Geology*, 44, 139-142, doi: 10.1130/G37490.

492 Latham, A.G., Schwarcz, H.P, Ford, D.C., 1986. The paleomagnetism and U-Th dating of Mexican
493 Stalagmite, Das2. *Earth Planetary Science Letters*, 79, 195-207.

494 Latham, A. G., Ford, D.C., Schwarcz, H.P., Birchall, T., 1989. Secular variation from Mexican
495 stalagmites: Their potential and problems. *Physics of the Earth and Planetary Interiors*, 56,
496 34–48.

497 Lean, C.B., Latham, A.C., Shaw, J., 1995. Palaeosecular variation from a Vancouver Island
498 Stalagmite and comparison with Contemporary North American records. *J. Geomag.*
499 *Geoelectr.*, 47, 71-87.

500 Leonhardt, R., 2006. Analyzing rock magnetic measurements: The RockMagAnalyzer 1.0 software.
501 *Computers & Geosciences*, 32, 1420-1431.

502 Lowrie, W., 1990. Identification of ferromagnetic minerals in a rock by coercivity and unblocking
503 temperature properties. *Geophysical Research Letters*, 17, 159-162.

504 Malfatti, J., Principe, C., Gattiglia, G., 2011. Archeomagnetic investigation of a metallurgical
505 furnace in Pisa (Italy). *Journal of Cultural Heritage*, 12, 1-10.

506 Manda, M., Olsen, N., 2009. Geomagnetic and Archeomagnetic Jerks: Where Do We Stand? *Eos*,
507 *Transactions, American Geophysical Union*, 90, 24, 208-208.

508 Maxbauer, D.P., Feinberg, J.M., Fox, D.L., 2016. MAX UnMix: A web application for unmixing
509 magnetic coercivity distributions. *Computers & Geosciences*, 95, 140-145.

510 Morinaga, H., Inokuchi, H., Yaskawa, K., 1989. Palaeomagnetism of stalagmites (speleothems) in
511 SW Japan. *Geophys. J.*, 96, 519-528.

512 Nilsson, A., Holme, R., Korte, M., Suttie, N., Hill, M., 2014. Reconstructing Holocene geomagnetic
513 field variation: new methods, models and implications. *Geophysical Journal International*,
514 198, 1, 229-248.

515 Noel, M., Batt, C.M., 1990. A method for correcting geographically separated remanence
516 directions for the purpose of archaeomagnetic dating. *Geophysical Journal International*,
517 102, 753-756.

518 Openshaw, S., Latham, A., Shaw, J., 1997. Speleothem Palaeosecular Variation Records from
519 China: Their contribution to the coverage of Holocene Palaeosecular Variation Data in East
520 Asia. *J. Geomag. Geoelectr.*, 49,485-505.

521 Osete, M. L., Martin-Chivelet, J., Rossi, C., Edwards, R.L., Egli, R., Munoz-Garcia, M.B., Wang, X.F.,
522 Pavon-Carrasco, F.J., Heller, F., 2012. The Blake geomagnetic excursion recorded in a
523 radiometrically dated speleothem. *Earth Planetary Science Letters*, 353, 173–181.

524 Pan, Y., Zhu, R., Banerjee, S.K., Gill, J., Williams, Q., 2000. Rock magnetic properties related to
525 thermal treatment of siderite: behaviour and interpretation. *Journal of Geophysical*
526 *Research*, 105, 783-794.

527 Pavón-Carrasco, F.J., Osete, M.L., Torta, J.M., De Santis, A., 2014. A geomagnetic field model for
528 the Holocene based on archaeomagnetic and lava flow data. *Earth Planetary Science Letters*,
529 388, 98 - 109.

530 Perkins, A.M., 1996. Observations under microscopy of magnetic minerals extracted from
531 speleothems. *Earth and Planetary Science Letters*, 139, 281-289.

532 Ponte, J., Font, E., Veiga-Pires, C., Hillaire, M.C., 2016. Paleomagnetism in speleothems: Influence
533 of calcite growth dip on the natural remanent magnetization. *EGU General Assembly 2016*,
534 17-22 April, Vienna, p.7199

535 Richards, D.A., Dorale, J.A., 2003. Uranium-series chronology and environmental applications of
536 speleothems. *Review in Mineralogy and Geochemistry*, 52, 407-460.

537 Rolph, T.C., Vigliotti, L., Oldfield, F. 2004. Mineral magnetism and geomagnetic secular variation of
538 marine and lacustrine sediments from central Italy: timing and nature of local and regional
539 Holocene environmental change. *Quaternary Science Review*, 23, 1699–1722.

540 Scholz, D., Hoffmann, D.L., Hellstrom, J., Bronk Ramsey, C., 2012. A comparison of different
541 methods for speleothem age modelling. *Quaternary Geochronology*. 14, 94–104.

542 Strauss, B.E., Strehlau, J.H., Lascu, I., Dorale, J.A., Penn, R.L., Feinberg, J.M., 2013. The origin of
543 magnetic remanence in stalagmites: observations from electron microscopy and rock
544 magnetism. *Geochemistry Geophysics Geosystems*, 14, doi: 10.1002/2013GC004950

545 Symons, D.T.A., Cioppa, M.T., 2000. Crossover Plots: a useful method for plotting SIRM data in
546 paleomagnetism. *Geophysical Research Letters*, 27 (12), 1779-1782.

547 Tema, E., 2011. Archaeomagnetic Research in Italy: Recent achievements and future perspectives.
548 In: *The Earth's Magnetic Interior*, IAGA Special Sopron Book Series, Volume 1, Chapter 15,
549 pp. 213-233. Eds: Petrovsky, E., Herrero-Bervera, E., Harinarayana, T., Ivers, D., Springer, doi:
550 10.1007/978-94-007-0323-0_15.

551 Tema, E., Hedley, I., Lanos, Ph., 2006. Archaeomagnetism in Italy: A compilation of data including
552 new results and a preliminary Italian Secular Variation curve. *Geophysical Journal*
553 *International*, 167, 1160-1171.

554 Tema, E., Fantino, F., Ferrara, E., Lo Giudice, A., Morales, J., Goguitchaichvili, A., Camps, P., Barello,
555 F., Gulmini, M., 2013. Combined archaeomagnetic and thermoluminescence study of a brick
556 kiln excavated at Fontanetto Po (Vercelli, Northern Italy). *J. Arch. Science*, 40 (4), 2025-2035.

557 Tema, E., Camps, P., Ferrara, E., Poidras, T., 2015. Directional results and absolute
558 archaeointensity determination by the classical Thellier and the multi-specimen DSC
559 protocols for two kilns excavated at Osterietta, Italy. *Studia Geophysica Geodaetica*, 59, 554-
560 577.

561 Tema, E., Ferrara, E., Camps, P., Conati Barbaro, C., Spatafora, S., Carvallo, C., Poidras, Th., 2016.
562 The Earth's magnetic field in Italy during the Neolithic period: New data from the Early
563 Neolithic site of Portonovo (Marche, Italy). *Earth and Planetary Science Letters*, 448, 49-61.

564 Turner, G.M., Thompson, E., 1981. Lake sediment record of the geomagnetic secular variation in
565 Britain during Holocene times. *Geophysical Journal of the Royal Astronomical Society*, 65 (3),
566 703-725.

567 Vigliotti, L., 2006. Secular variation record of the Earth's magnetic field in Italy during the
568 Holocene: constraints for the construction of a master curve. *Geophys. J. Int.*, 165, 414–429.

569 Xie, S., Evershed, R.P., Huang, X., Zhu, Z., Pancost, R.D., Meyers, P.A., Gong, L., Hu, C., Huang, J.,
570 Zhang, S., Gu, Y., Zhu Y., 2013. Concordant monsoon-driven postglacial hydrological changes
571 in peat and stalagmite records and their impacts on prehistoric cultures in central China.
572 *Geology*, 41, 827-830, doi:10.1130/G34318.1

573 Zhu, Z., Zhang, S., Tang, C., Li, H., Xie, S., Ji, J., Xiao, G., 2012. Magnetic fabric of stalagmites and its
574 formation mechanism. *Geochemistry Geophysics Geosystems*, 13, doi:
575 10.1029/2011GC003869.

576

577 **Figure Caption**

578

579 Figure 1. a) Structural sketch map of the Western Alps; b) 3D reconstruction of the Inner Western
580 Alps in the Rio Martino zone (modified after Balestro et al., 2014). The square indicates the
581 location of the Rio Martino Cave. Note: the region highlighted in the small inset map is not the
582 same as the one shown in the enlargement.

583 Figure 2. a) Part of core RMD8; b) part of the flowstone systematically cut and sampled in 3 mm-
584 thick slices; c) the amagnetic plastic cylindrical holder created in order to fix the small samples in
585 the centre of the cylinder and treat them as standard paleomagnetic samples.

586 Figure 3. Age-depth model for RMD1 core. The age is expressed both in ka AD and in b2k (before 2
587 ka).

588 Figure 4. The distribution of the mineral species in the insoluble (detrital) fraction of Rio Martino
589 speleothem. The picture is the sum of ca 1500 EDS determinations from seven different portions
590 from the same core. The “accessory minerals” are species <2.5 % of the analyzed particles, for
591 each sample and includes rutile, zircon, monazite, apatite (mainly apatite-F), sphene, xenotime,
592 galena, pyrite, ilmenite, barite.

593 Figure 5. a) Isothermal remanent magnetization (IRM) acquisition curves; b) thermal
594 demagnetization of a composite three-axes IRM (Lowrie, 1990); c) crossover plots (Symons and
595 Cioppa, 2000).

596 Figure 6. Equal area stereographic projections of the eigenvectors for a) the anisotropy of
597 magnetic susceptibility, and for b) and c) isothermal remanent magnetization, where the
598 maximum, intermediate, and minimum eigenvectors are denoted by squares, triangles, and
599 circles, respectively. The 95% confidence ellipses for the eigenvectors are shown by unfilled

600 ellipses. The mean ChRM directions and their α_{95} errors for specimens SP200 to SP260 (b) and
601 SP346 to SP397 (c) are denoted by stars with grey ellipses.

602 Figure 7. Thermal and AF demagnetization results from twin specimens from samples a-b) RM7
603 and c-d) RM20 plotted in intensity decay plots (left) and Zijderveld diagrams (right). Symbols: full
604 dots = declination; open dots = apparent inclination.

605 Figure 8. Equal-area projections of the ChRM directions for five samples obtained from a) AF and
606 b) thermal demagnetization on twin specimens. The star represents the mean value calculated for
607 each group of samples following a Fisherian distribution.

608 Figure 9. a) Declination and b) inclination data from cores RMD1 (red) and RMD8 (blue) plotted
609 versus depth in mm from the top of the core.

610 Figure 10. a) Declination and b) inclination plots of the RMD1 (red) and RMD8 (blue) compared
611 with the Italian archaeomagnetic data from archeological artefacts (green diamonds) and volcanic
612 rocks (black squares) and the pfm9k (magenta line) and SHA.DIF.14k (black line) global
613 geomagnetic field models. All directions are calculated at the geographic coordinates of Rio
614 Martino (44.7° N, 7.15° E). Age is given both as Calendar Age (year AD) and b2k (before 2 ka).

615 **Figure caption of the Supplemental material**

616 Figure S1. a) Photograph of the flowstone's sampling and b) of the device to orient the core.

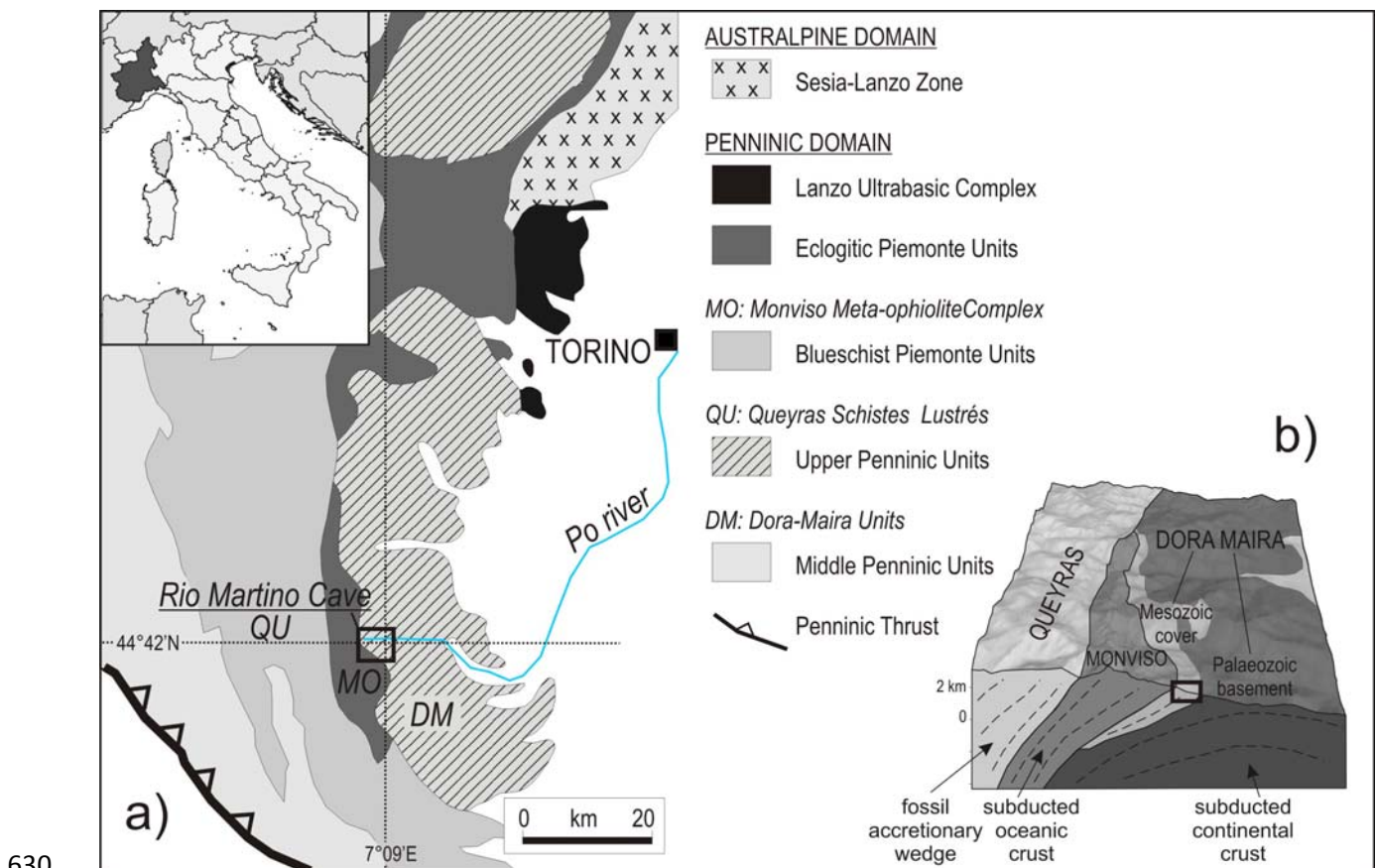
617 Figure S2. a) Mass susceptibility and b) mass remanence intensity from RMD1 (red) and RMD8
618 (blue) plotted versus depth in mm from the top of the core.

619 Figure S3. Hysteresis curves (mass magnetization versus applied field) for specimens SP421 and
620 SP460. In a) uncorrected curves; in b) slope-corrected for diamagnetic effect curves.

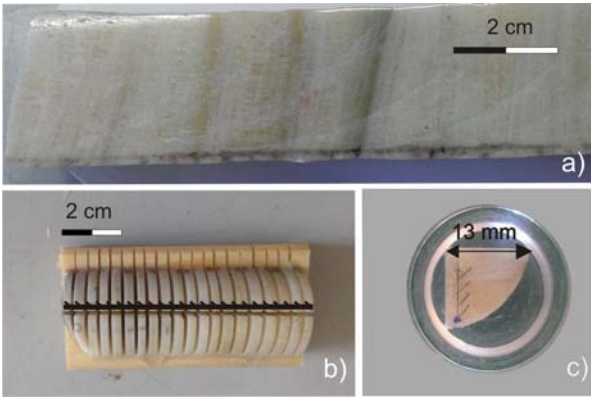
621 **Table caption**

622 Table S1. Corrected U/Th ages for RMD1 core. Isotope ratios are expressed as activity ratios
623 standardized to the HU-1 secular equilibrium standard. Ages have been calculated using decay
624 constants of 9.195×10^{-6} (^{230}Th) and 2.835×10^{-6} (^{234}U). Depths are from top.

625 Table S2. Characteristic remanent magnetization directions (ChRMs) of the samples from the
626 RMD1 (left) and RMD8 (right) cores. Legend: z = depth in mm from the core top; D, I = magnetic
627 declination and inclination; MAD = Mean Angular Deviation; D_{corr} = declination corrected by
628 subtracting the angular difference between the $D_{\text{GAD}} = 0^\circ$ and the mean ChRM declination ($D =$
629 146.1°).

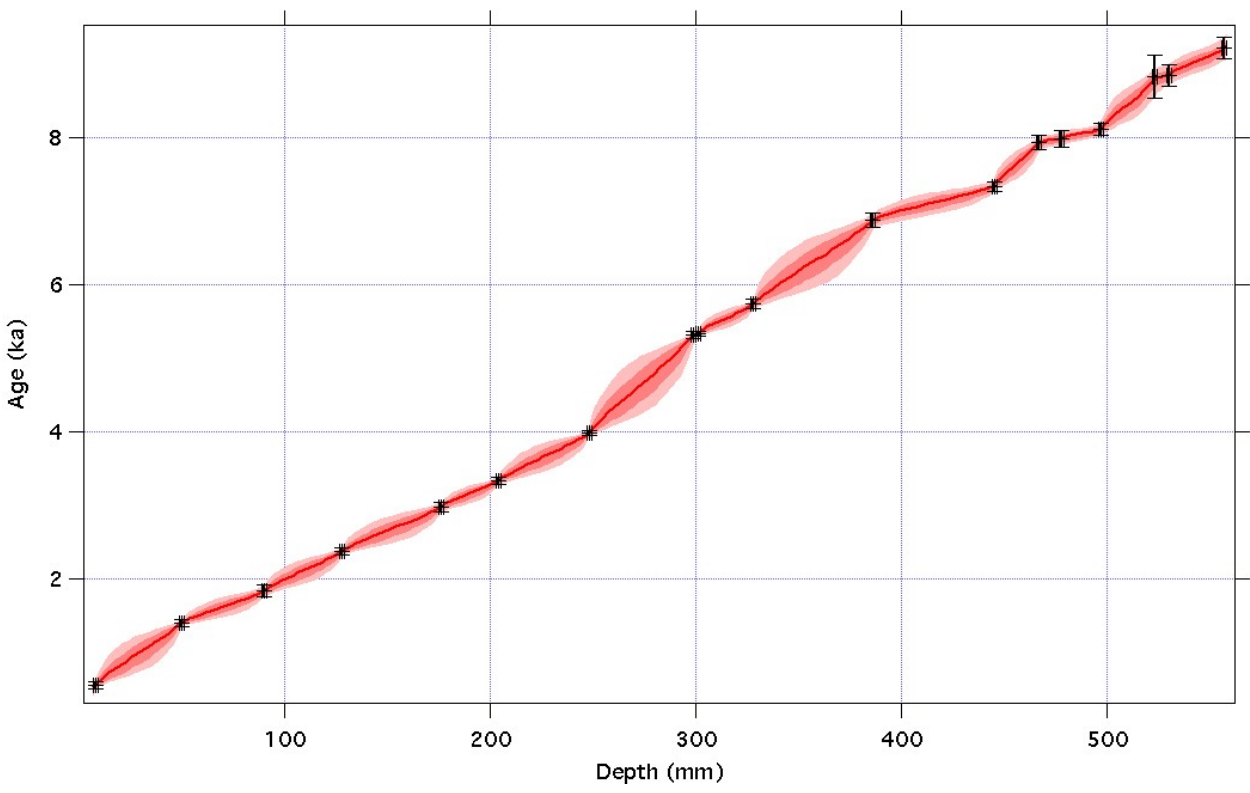


630
631 **Figure 1**



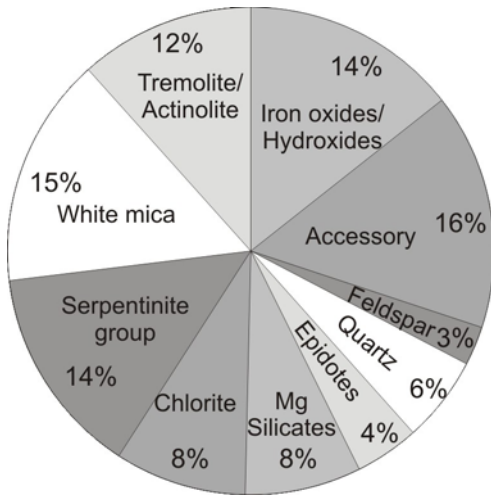
632

633 Figure 2



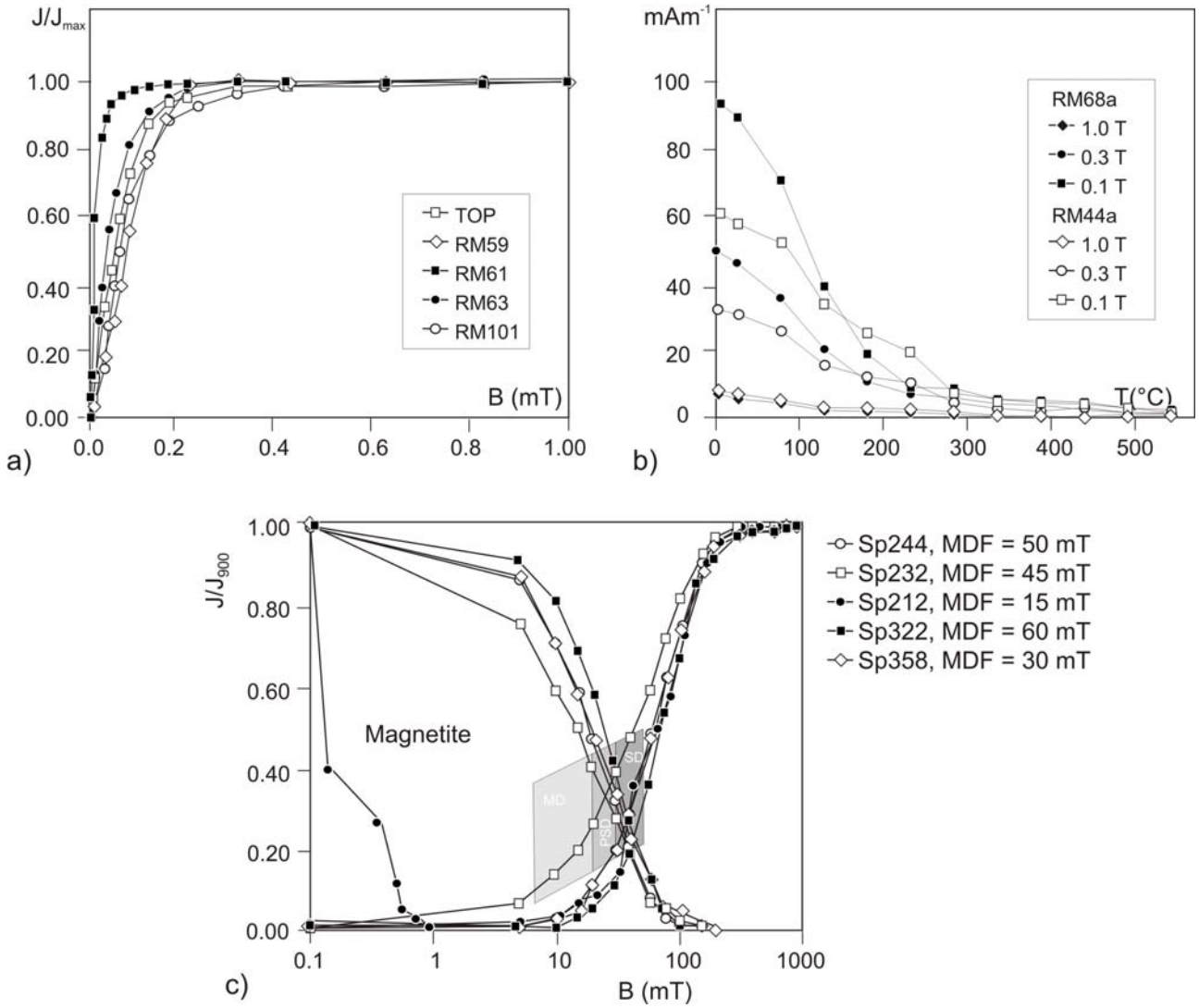
634

635 Figure 3



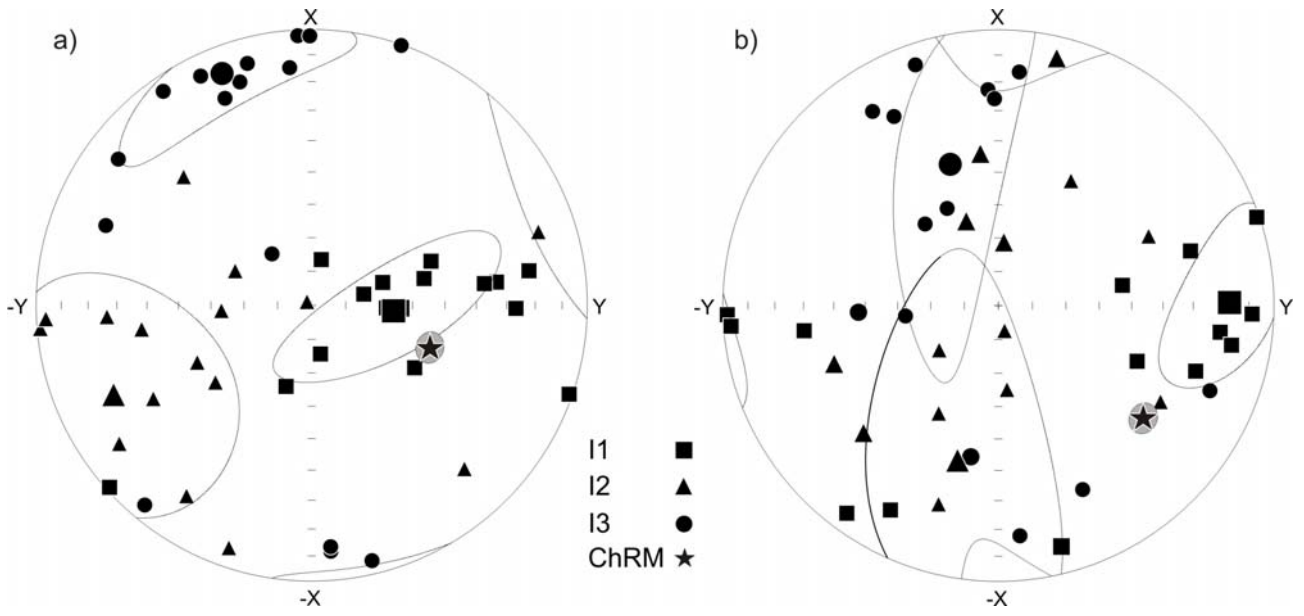
636

637 Figure 4



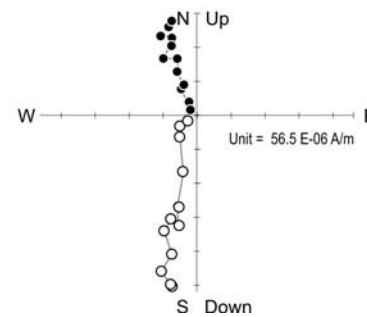
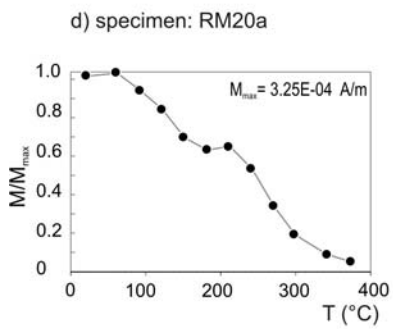
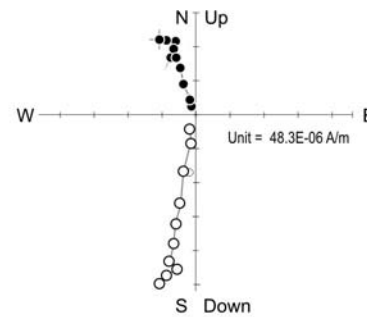
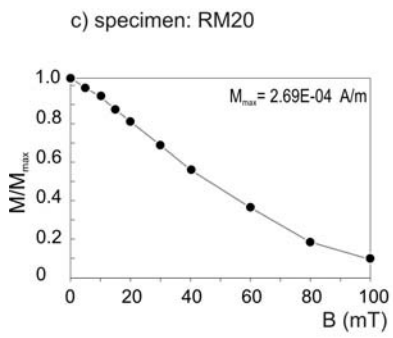
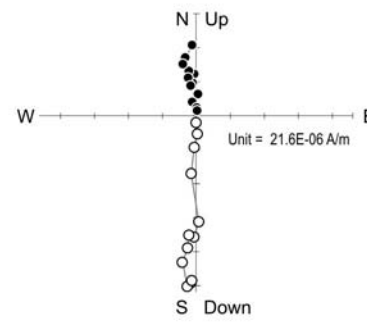
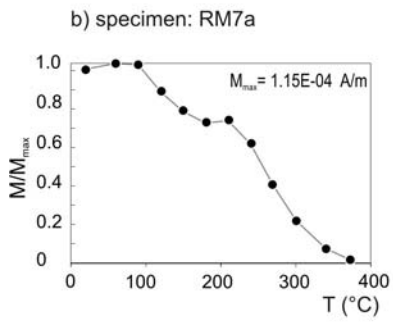
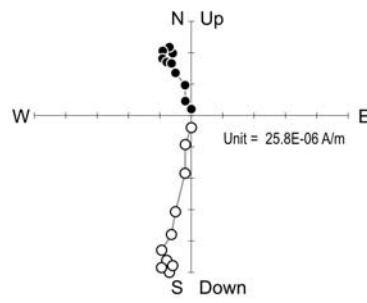
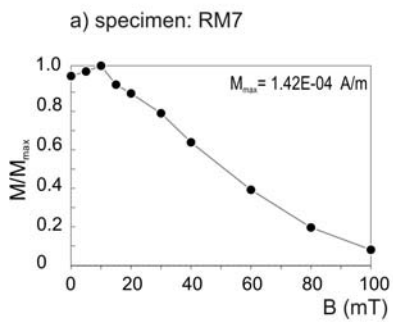
638

639 Figure 5



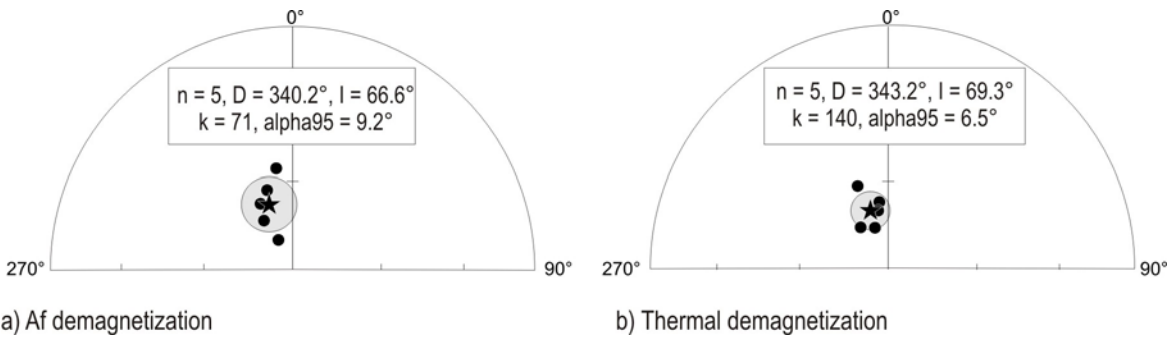
640

641 Figure 6



642

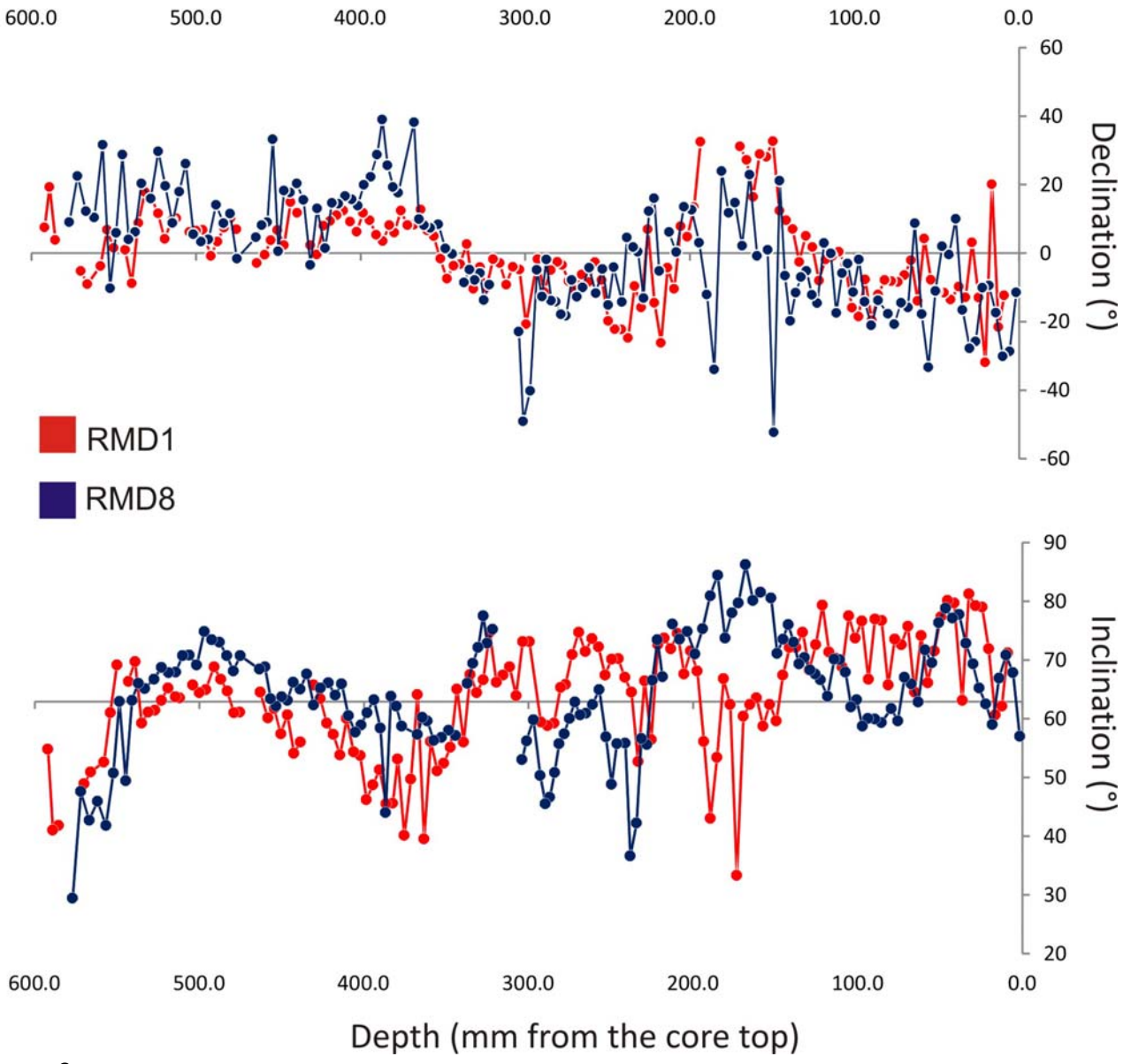
643 Figure 7



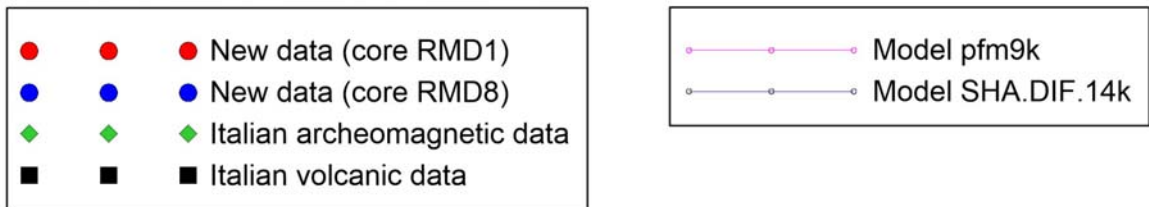
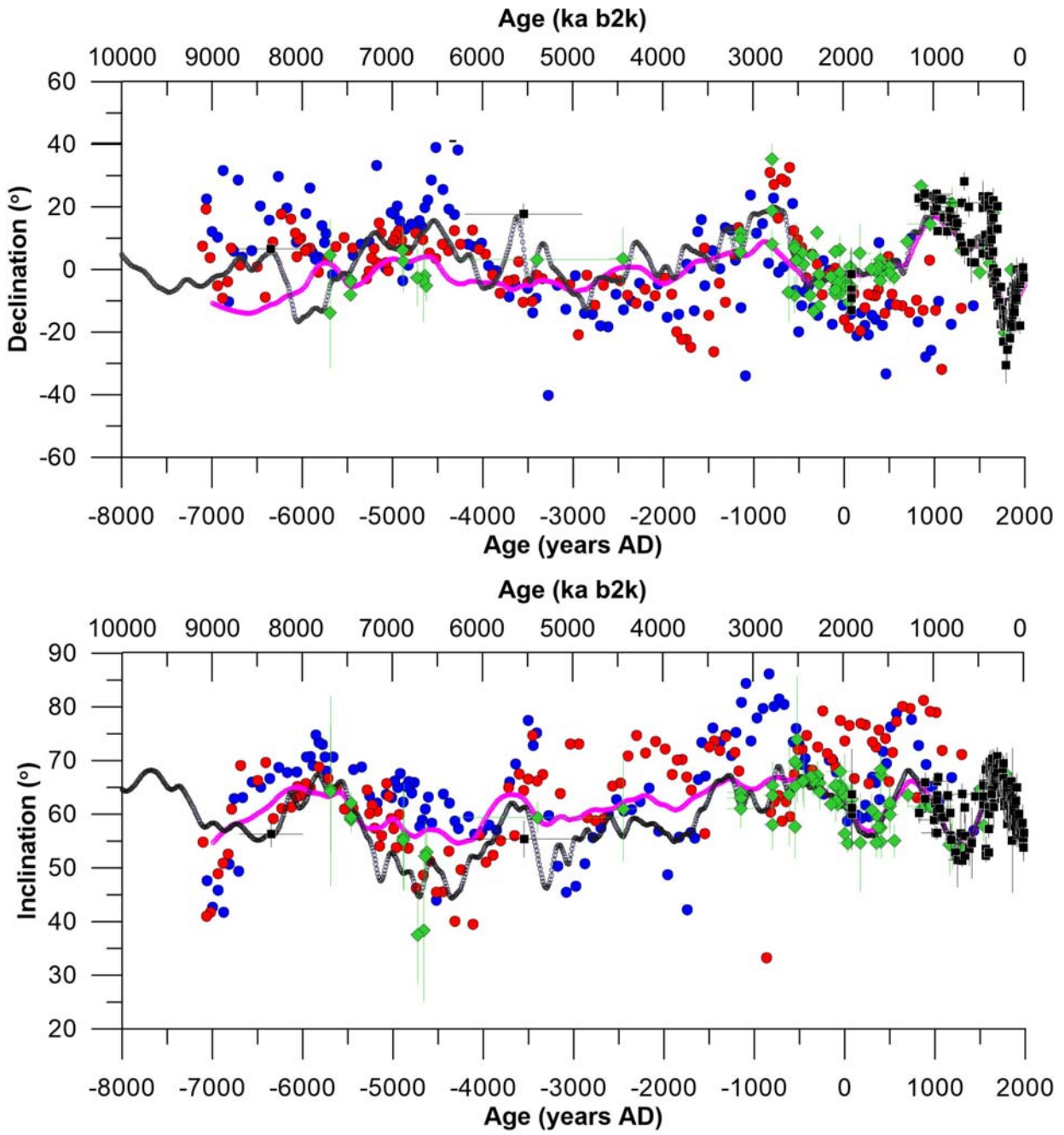
644 a) Af demagnetization

b) Thermal demagnetization

645 Figure 8



646
647 Figure 9



648

649 Figure 10

650